

• Supplementary File •

## Multi-wavelength plasmonic optoelectronic memristor for reconfigurable logic operations and mixed-color pattern recognition

Jiaqi Han<sup>1</sup>, Zhuangzhuang Li<sup>1</sup>, Tao Zeng<sup>2</sup>, Xuanyu Shan<sup>1</sup>, Riya Su<sup>1</sup>, Ya Lin<sup>1</sup>, Zhongqiang Wang<sup>1\*</sup>, Xiaoning Zhao<sup>1</sup>, Shencheng Fu<sup>1</sup>, Haiyang Xu<sup>1</sup> & Yichun Liu<sup>1\*</sup>

<sup>1</sup>*Key Laboratory for UV Light-Emitting Materials and Technology (Northeast Normal University),  
Ministry of Education, 5268 Renmin Street, Changchun, China;*

<sup>2</sup>*Department of Materials Science and Engineering, National University of Singapore, Singapore 117575, Singapore*

---

\* Corresponding author (email: wangzq752@nenu.edu.cn, ycliu@nenu.edu.cn)

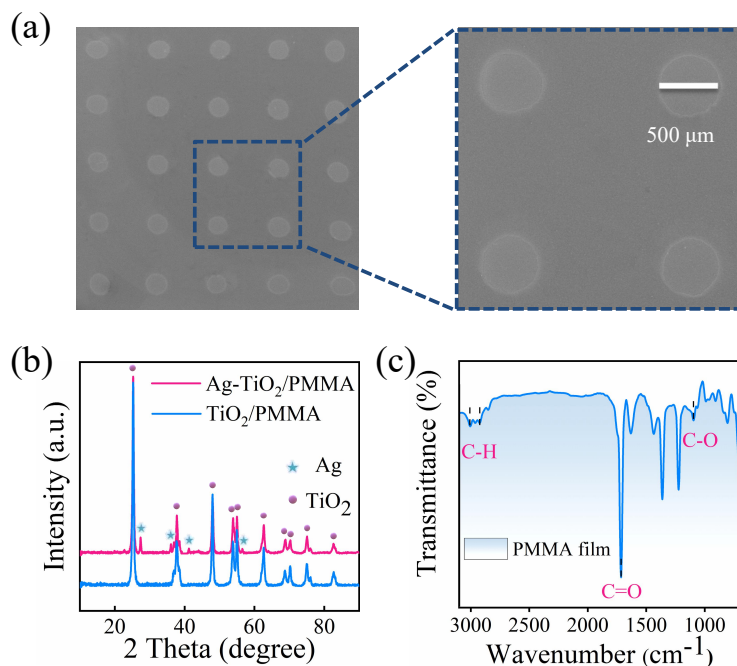


**Figure S1** Structural characterization of plasmonic optoelectronic memristor based on Ag-TiO<sub>2</sub>/PMMA nanocomposite. (a) The top view SEM image of the Au/Ag-TiO<sub>2</sub>/PMMA/FTO memory cell. (b) Fourier-transform infrared spectra of the PMMA film. (c) X-ray diffraction patterns of TiO<sub>2</sub>/PMMA and Ag-TiO<sub>2</sub>/PMMA composites.

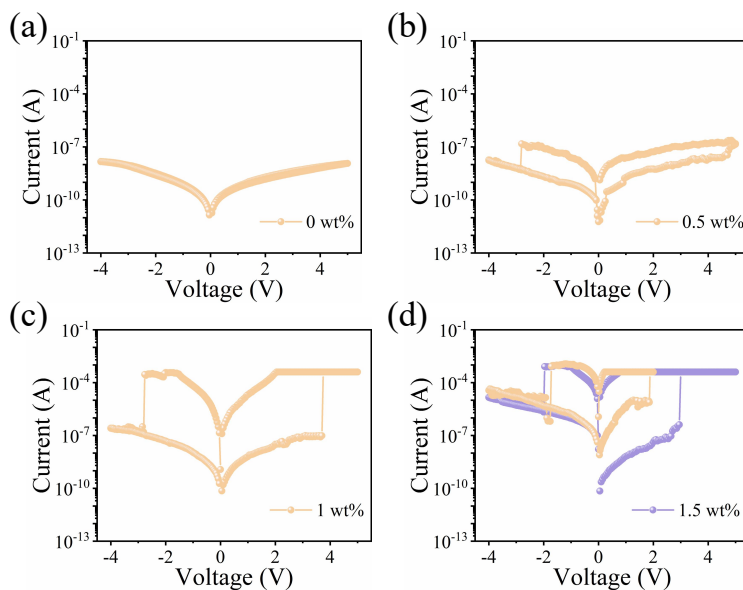


**Figure S2** The effect of Ag-TiO<sub>2</sub> concentration on the RS behaviors. Herein, the concentration of titanium dioxide coated Ag nanoparticles were (a) 0 wt% (b) 0.5 wt% (c) 1 wt% (d) 1.5 wt%, respectively.

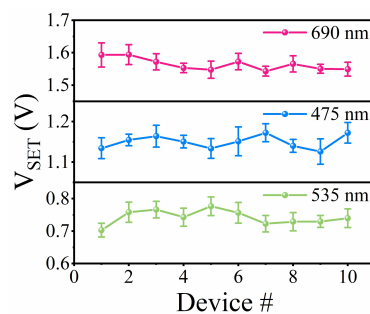


**Figure S3** The device-to-device values of V<sub>SET</sub> after visible light irradiation with different light wavelengths.

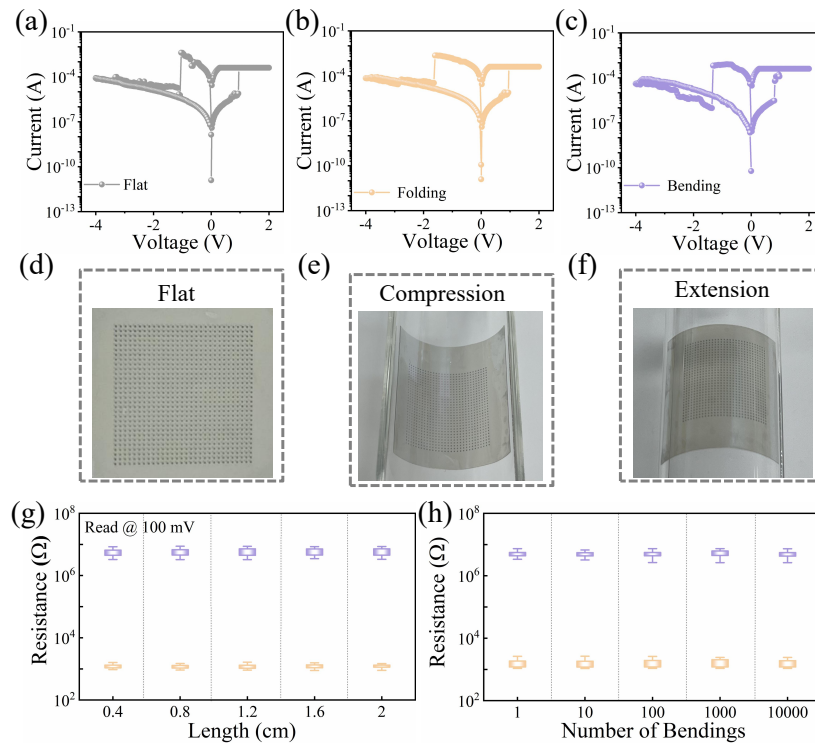


**Figure S4** I-V characteristic curve of the Au/Ag-TiO<sub>2</sub>/PMMA/FTO memory device. (a) flat, (b) folding, and (c) bending states. The corresponding photographs of the device in the (d) flat, (e) folding, and (f) bending states, respectively. (g) Statistical values of HRS/LRS under different bending lengths and (h) different bending times.

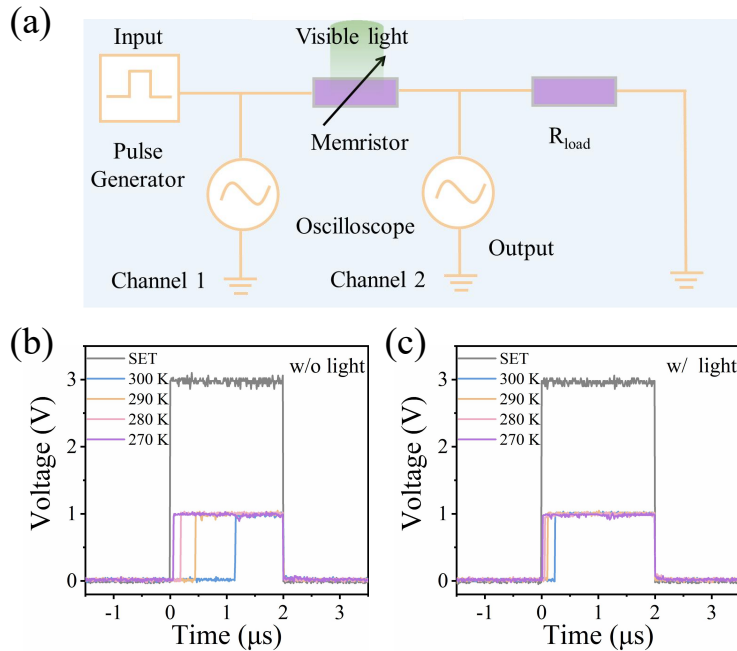


**Figure S5** The measurement of Ag-migration barrier of the Ag-TiO<sub>2</sub>/PMMA memory cells without/with visible light irradiation (the Ag-TiO<sub>2</sub> concentration was fixed at 1.5 wt%). (a) Schematic diagram of a test setup for electric-pulse-induced switching without/with light irradiation. (b, c) Typical response profiles to the applied set pulse as a function of temperature without light irradiation and with 535 nm light irradiation, respectively.

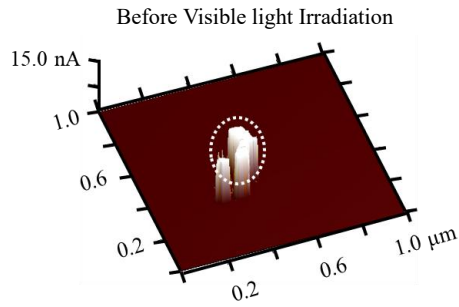


**Figure S6** Local conductivity of the Au/Ag-TiO<sub>2</sub>/PMMA/FTO memristor measured by C-AFM (10 mV bias) for the LRS state after SET operation in a dark environment.

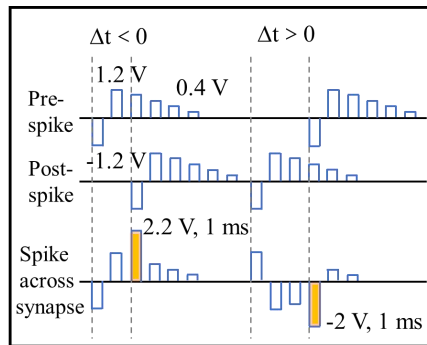


**Figure S7** The amplitude superposition method, where spike trains are designed to implement STDP by Au/Ag-TiO<sub>2</sub>/PMMA/FTO memristor. The spike amplitudes for the pre- and postspikes are -1.2, 1.2, 1, 0.8, 0.6, and 0.4 V, consecutively. The spike duration and interval were 1 ms in this experiment.

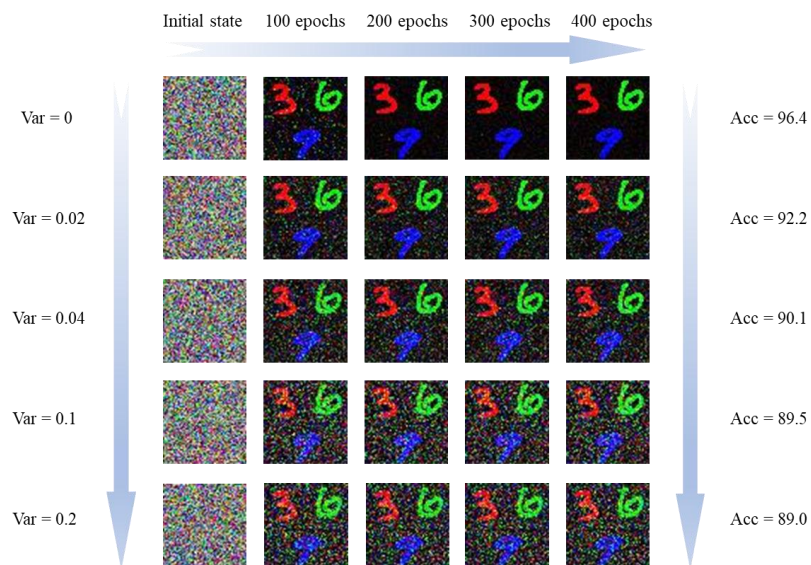


**Figure S8** Evolution of images during the learning process based on Au/Ag-TiO<sub>2</sub>/PMMA/FTO devices with different variance deviation noise to demonstrate the fault-tolerance capability of our neuromorphic visual system.